Superhydrophilic CuO nanowires QCM humidity sensors with horsefly-inspired self-cleaning ability applied on non-contact detection

Chengxu Lin[1, †], Chunhua He[1, †], Jianbin Lin[1], Chenyu Li[1], Bo Sun[2], Shilong Peng[3], Lingxian Kong[1], Shuang Xi[3], Zhiyong Liu[1, *], Guanglan Liao[1, *], Tielin Shi[1]

[1]State Key Laboratory of Intelligent Manufacturing Equipment and Technology, Huazhong University of Science and Technology, Wuhan 430074, China.

[2]School of Aerospace Engineering, Huazhong University of Science and Technology, Wuhan 430074, China.

[3]College of Mechanical and Electronic Engineering, Nanjing Forestry University, Nanjing 210037, China

[*]Corresponding authors. E-mail: zhiyong_liu@hust.edu.cn, guanglan.liao@hust.edu.cn

[†]Co-first authors. These authors contributed equally to this work.

This file includes:

Figs. S1 to S23
Tables S1 to S4

Other Supplementary Materials for this manuscript include the following:

Movies S1 to S3

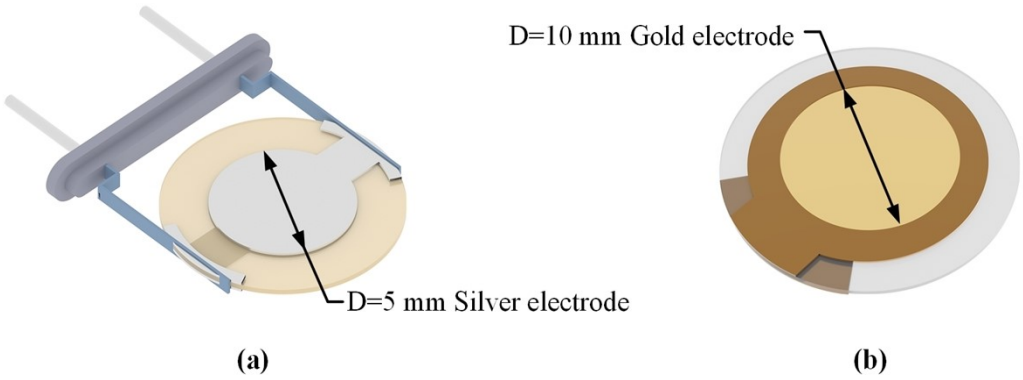

Fig. S1. (**a**) Structure of bare QCMs with an AT crystal (8 mm in diameter) and two silver electrodes (5 mm in diameter); (**b**) Structure of bare QCMs with an AT crystal (15 mm in diameter) and two gold electrodes (10 mm in diameter).

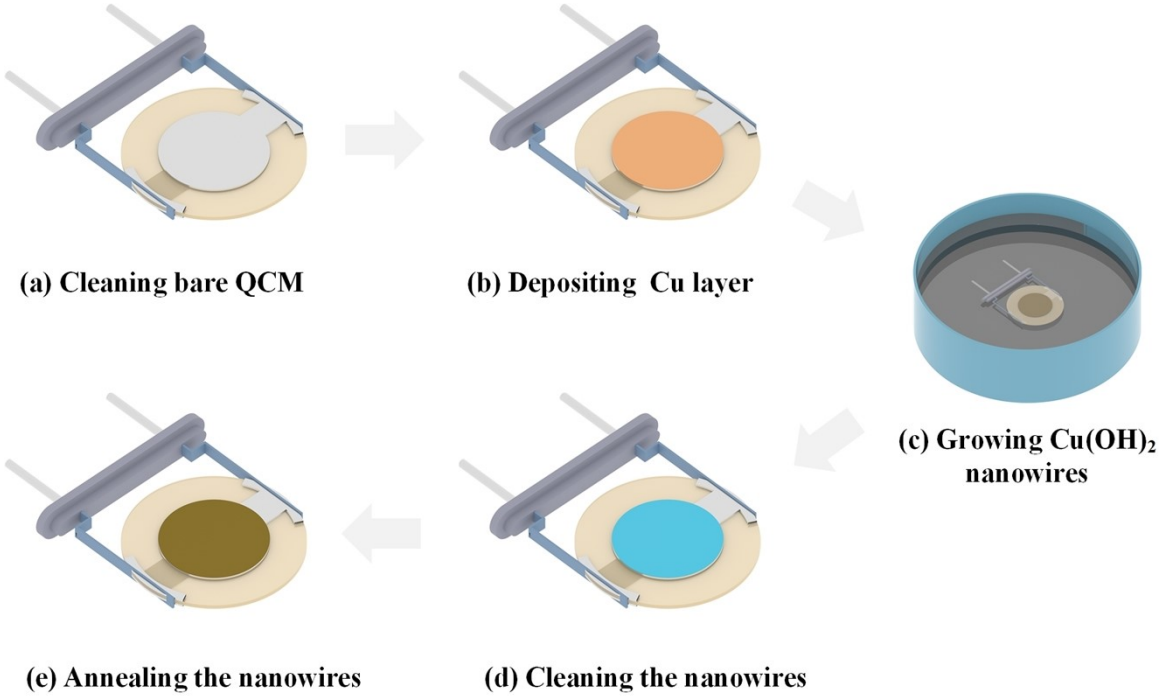

Fig. S2. Flow protocols of the fabrication for CuO nanowires based QCMs. (**a**) Cleaning bare QCMs, (**b**) depositing Cu layer, (**c**) in-situ growing the $Cu(OH)_2$ nanowires in solution, (**d**) $Cu(OH)_2$ nanowires QCM humidity sensor, (**e**) in-situ annealing $Cu(OH)_2$ nanowires in air.

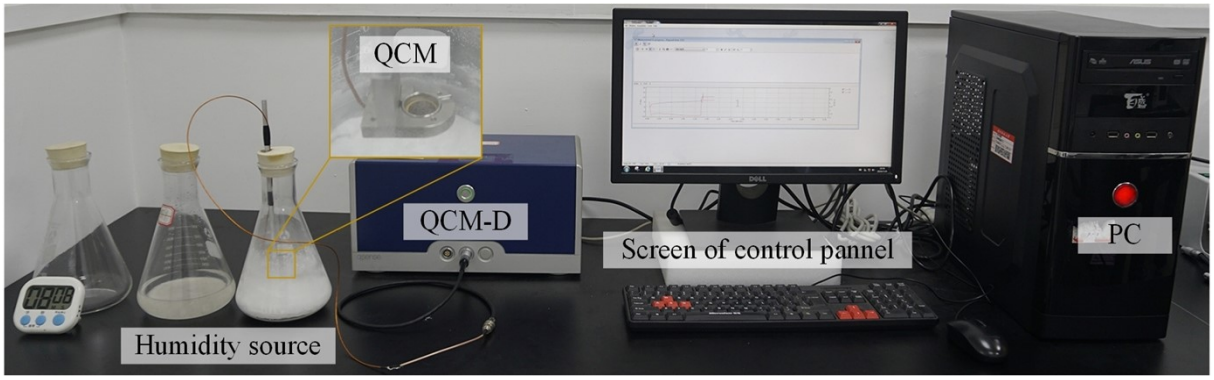

Fig. S3. Schematic diagram of the experimental setup for humidity detection by QCM-D.

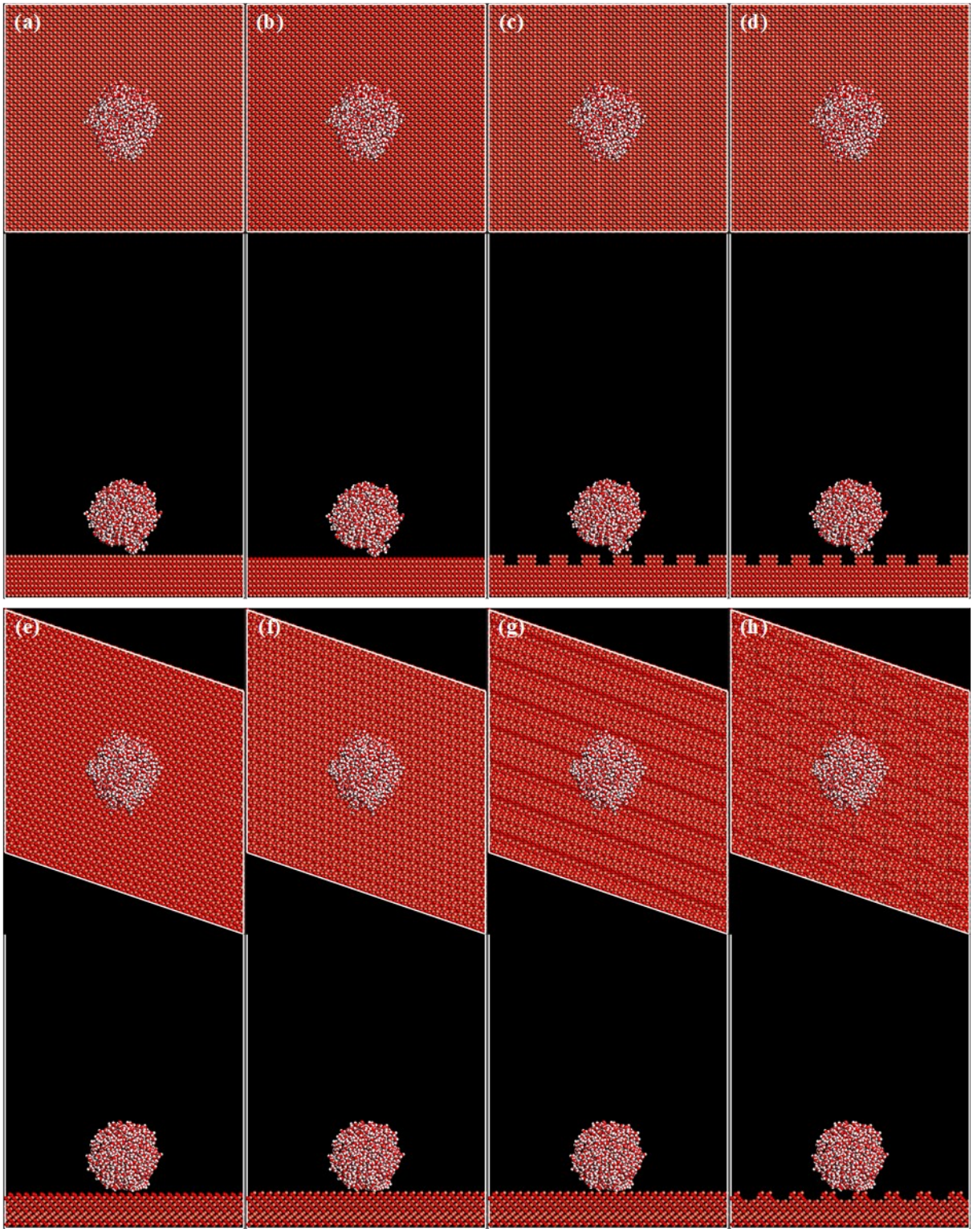

Fig. S4. Water droplet on CuO (111) surface (**a**) Cu; (**b**) O; (**c**) stripe groove; (**d**) vertical and horizontal groove; Water droplet on CuO (002) surface (**e**) Cu; (**f**) O; (**g**) stripe groove; (**h**) vertical and horizontal groove.

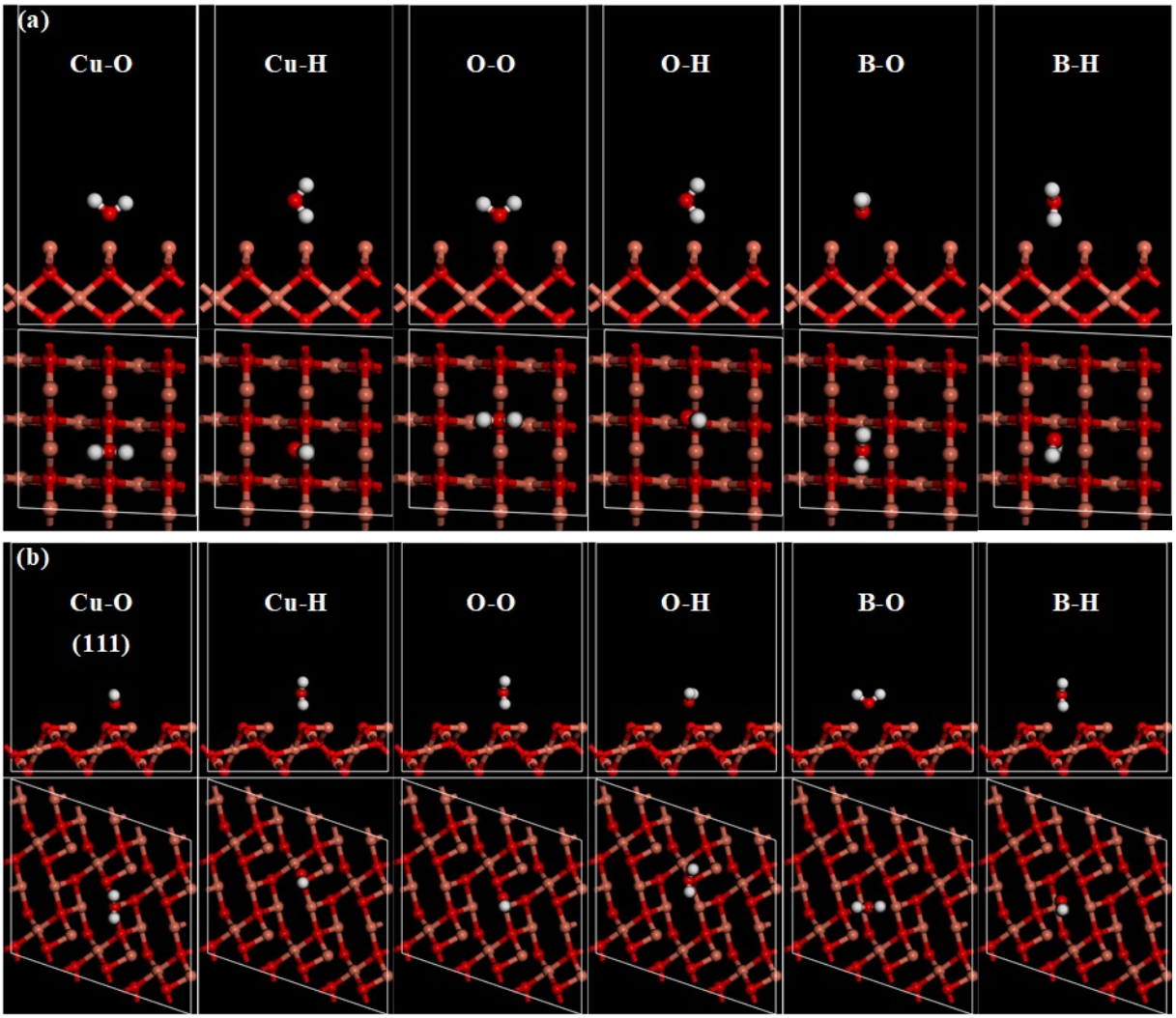

Fig. S5. Adsorption geometries of H_2O on the CuO surfaces. (**a**) (002); (**b**) (111). The salmon pink, red and gray balls represent Cu, O, and H atoms, respectively.

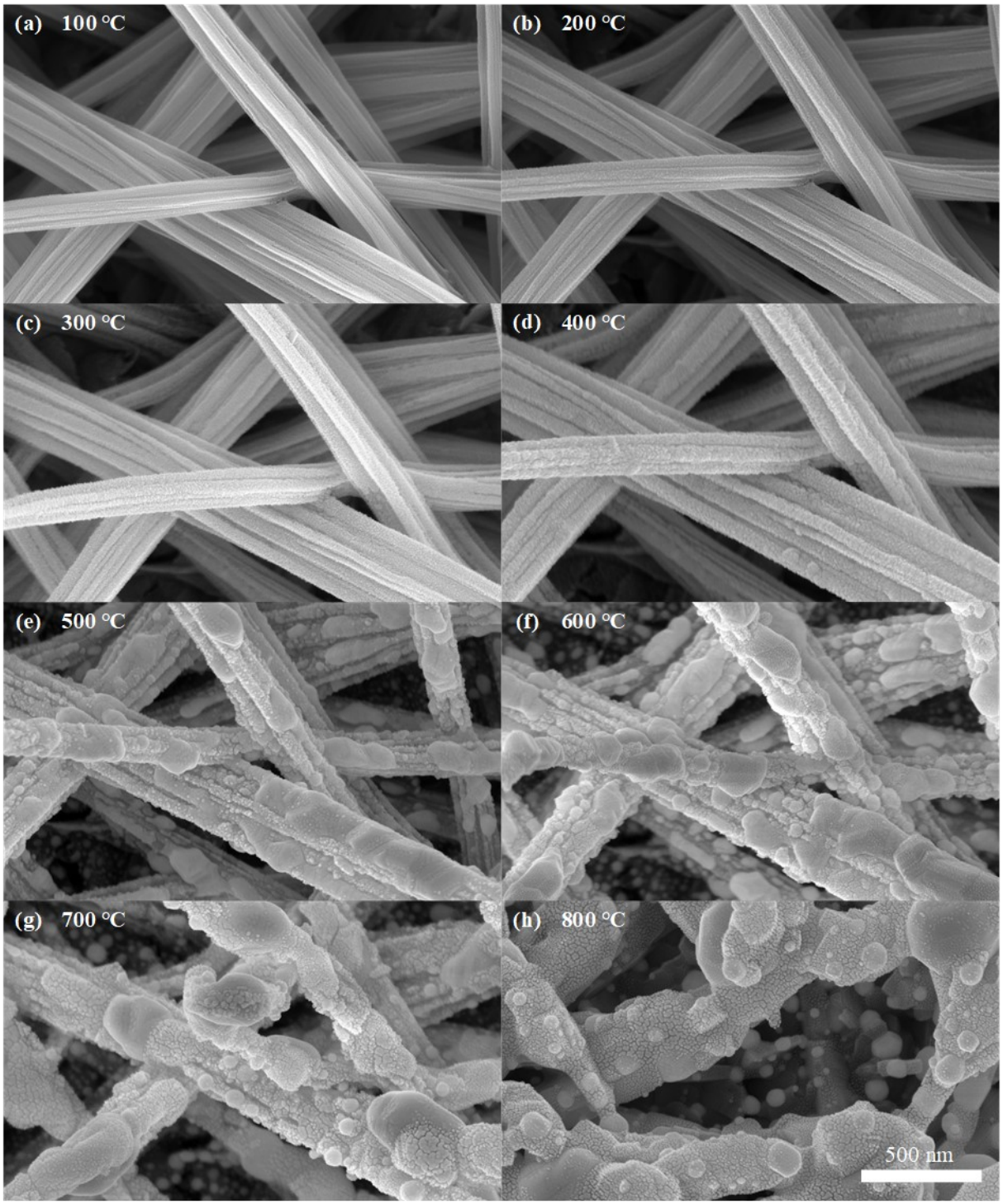

Fig. S6. The SEM images of the nanowires annealed at (**a**) 25°C, (**b**) 200°C, (**c**) 300°C, (**d**) 400°C, (**e**) 500°C, (**f**) 600°C, (**g**) 700°C, (**h**) 800°C last for 1 hour with a heating rate of 5 °C/min.

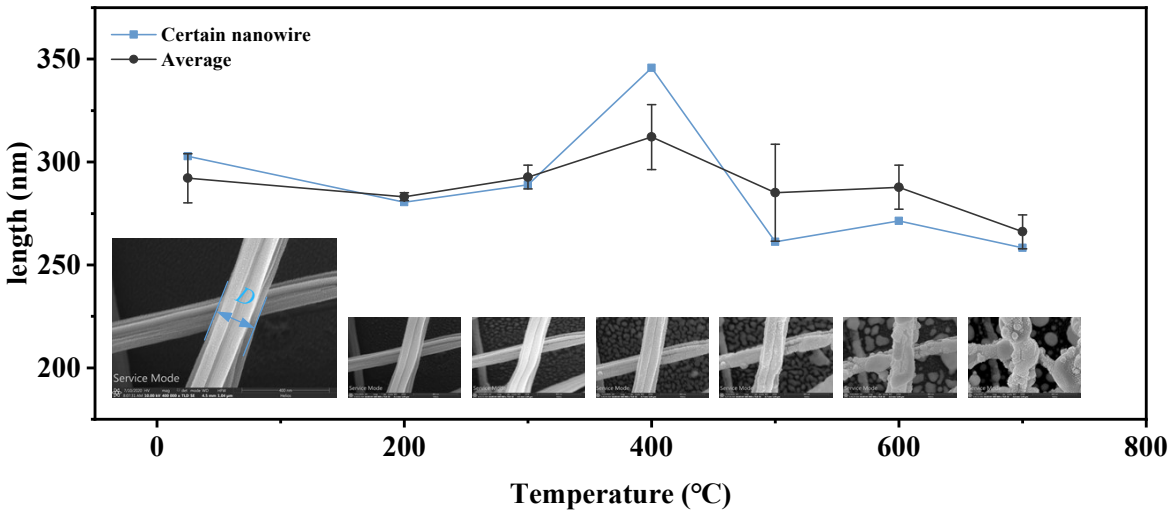

Fig. S7. The width of the nanowires *vs*. annealing temperature.

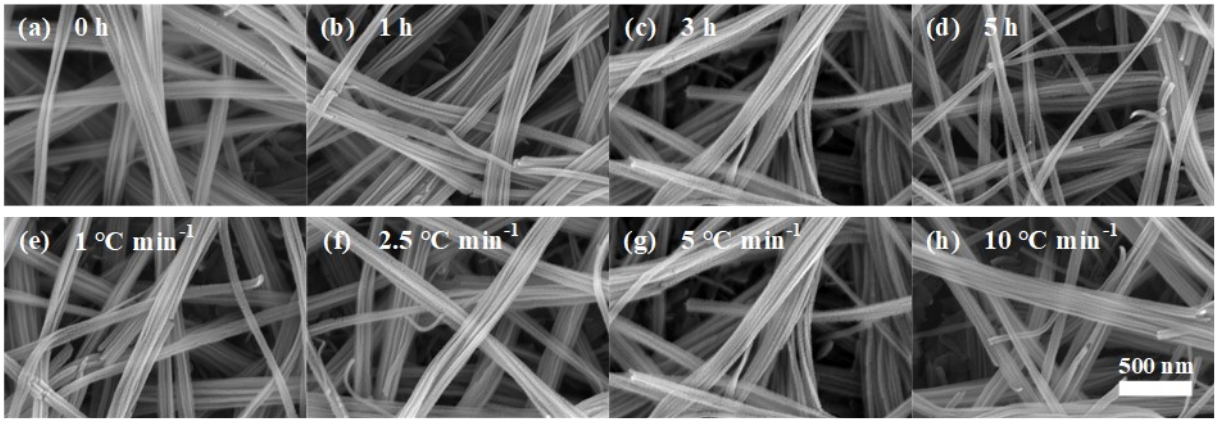

Fig. S8. SEM images of the CuO nanowires after annealing at 300 ℃ for (**a**) 0 h, (**b**) 1 h, (**c**) 3 h and (**d**) 5 h; at 300 ℃ for 3 h with a heating rate of (**e**) 1 ℃ min^{-1}, (**f**) 2.5 ℃ min^{-1}, (**g**) 5 ℃ min^{-1} and (**h**) 20 ℃ min^{-1}.

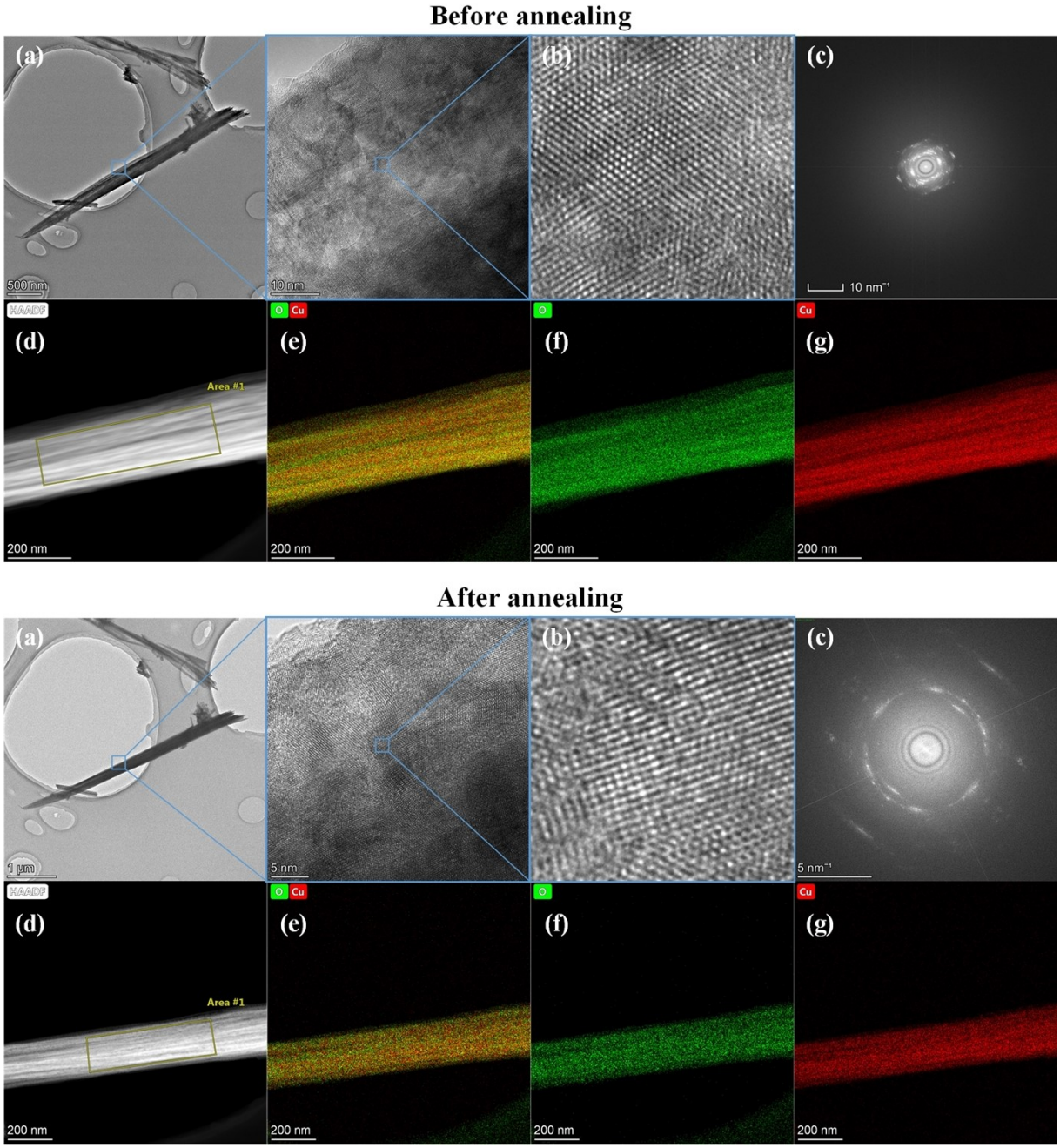

Fig. S9. TEM images，HRTEM images, SEAD images and Element mapping of the nanowires before and after annealing.

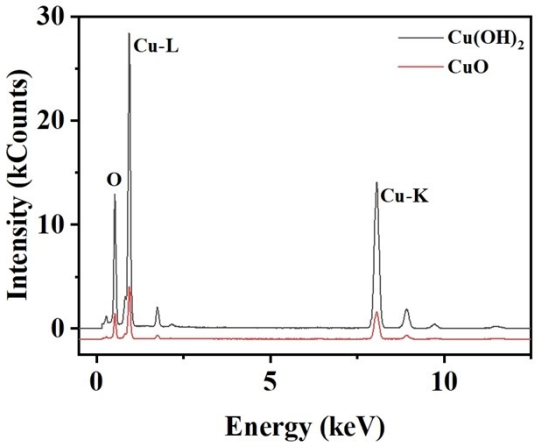

Fig. S10. EDS images of the nanowires before and after annealing.

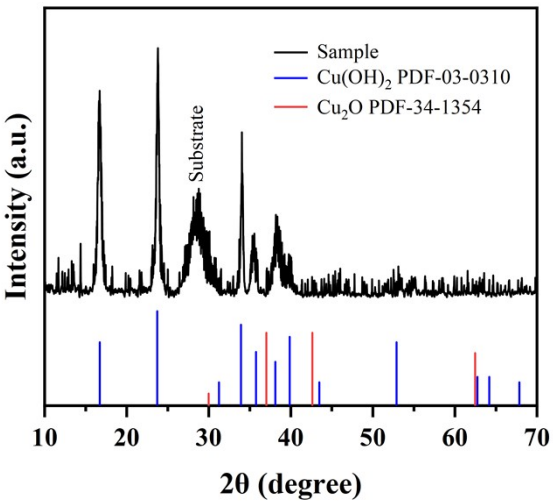

Fig. S11. XRD pattern of the $Cu(OH)_2$ nanowires before annealing.

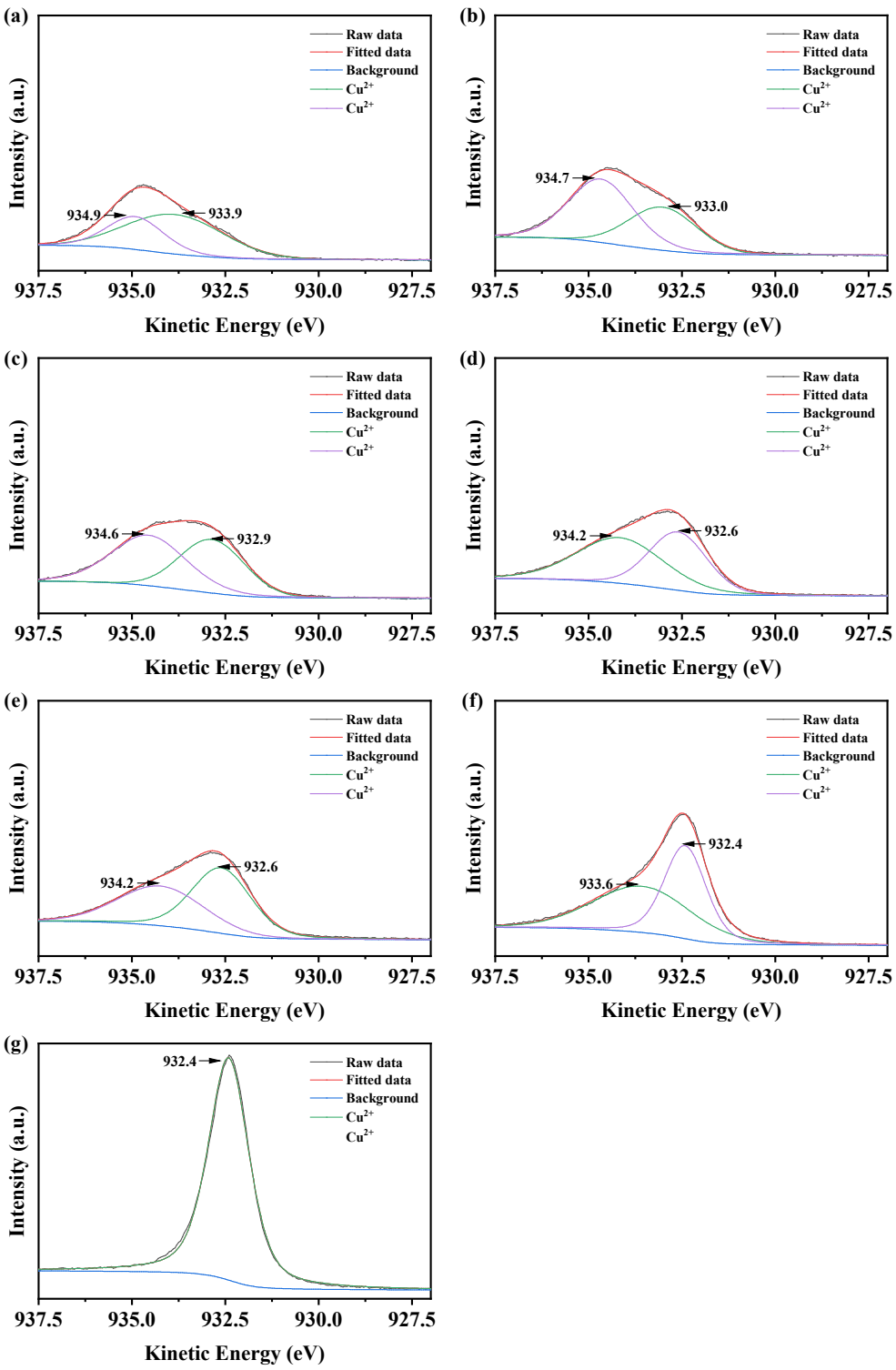

Fig. S12. XPS curves of Cu element of sensing materials at (**a**) 30℃; (**b**) 100℃; (**c**) 140℃; (**d**) 160℃; (**e**) 200℃; (**f**) 300℃; (**g**) 400℃.

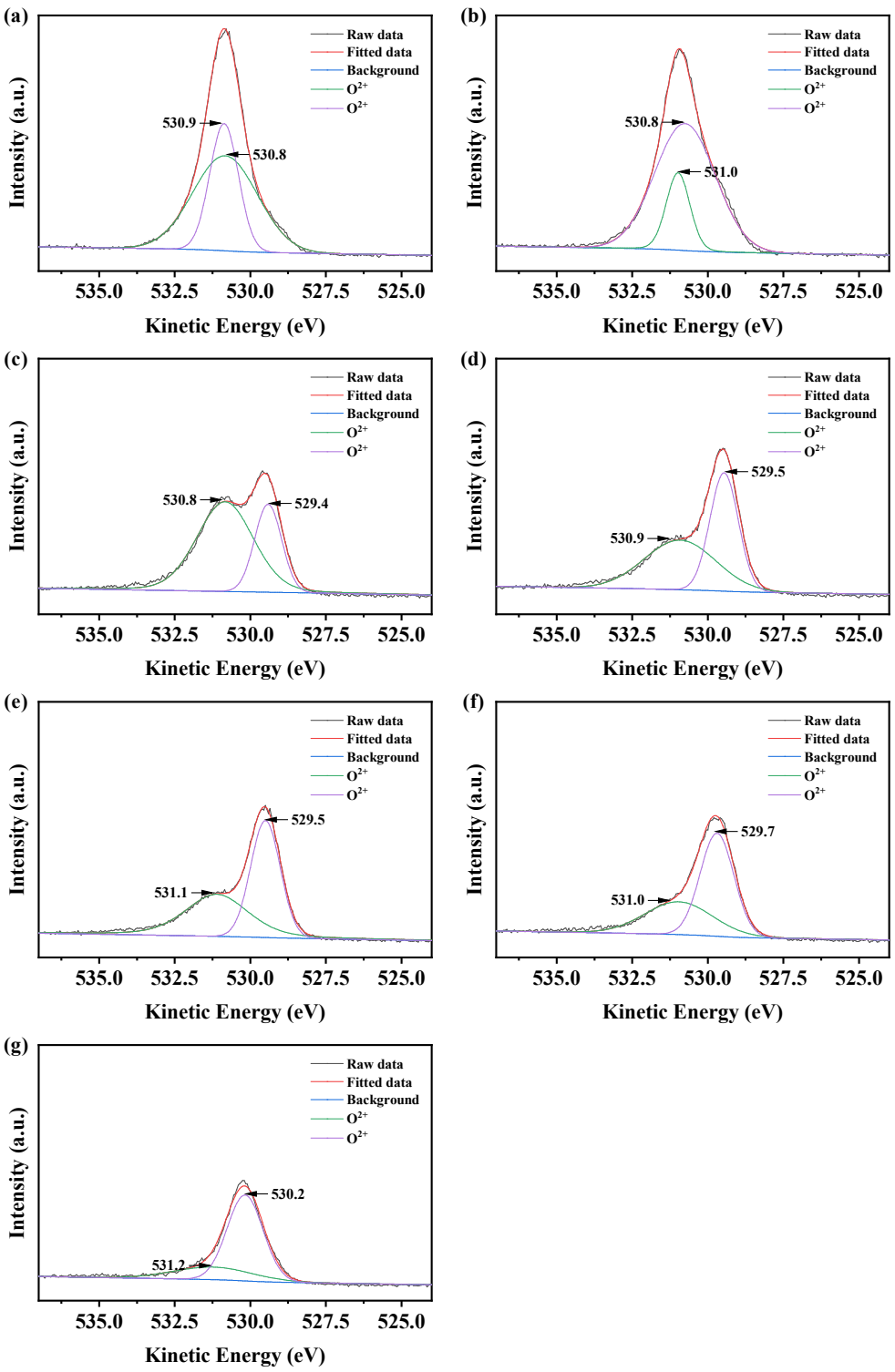

Fig. S13. XPS curves of O element of sensing materials at (**a**) 30℃; (**b**) 100℃; (**c**) 140℃; (**d**) 160℃; (**e**) 200℃; (**f**) 300℃; (**g**) 400℃.

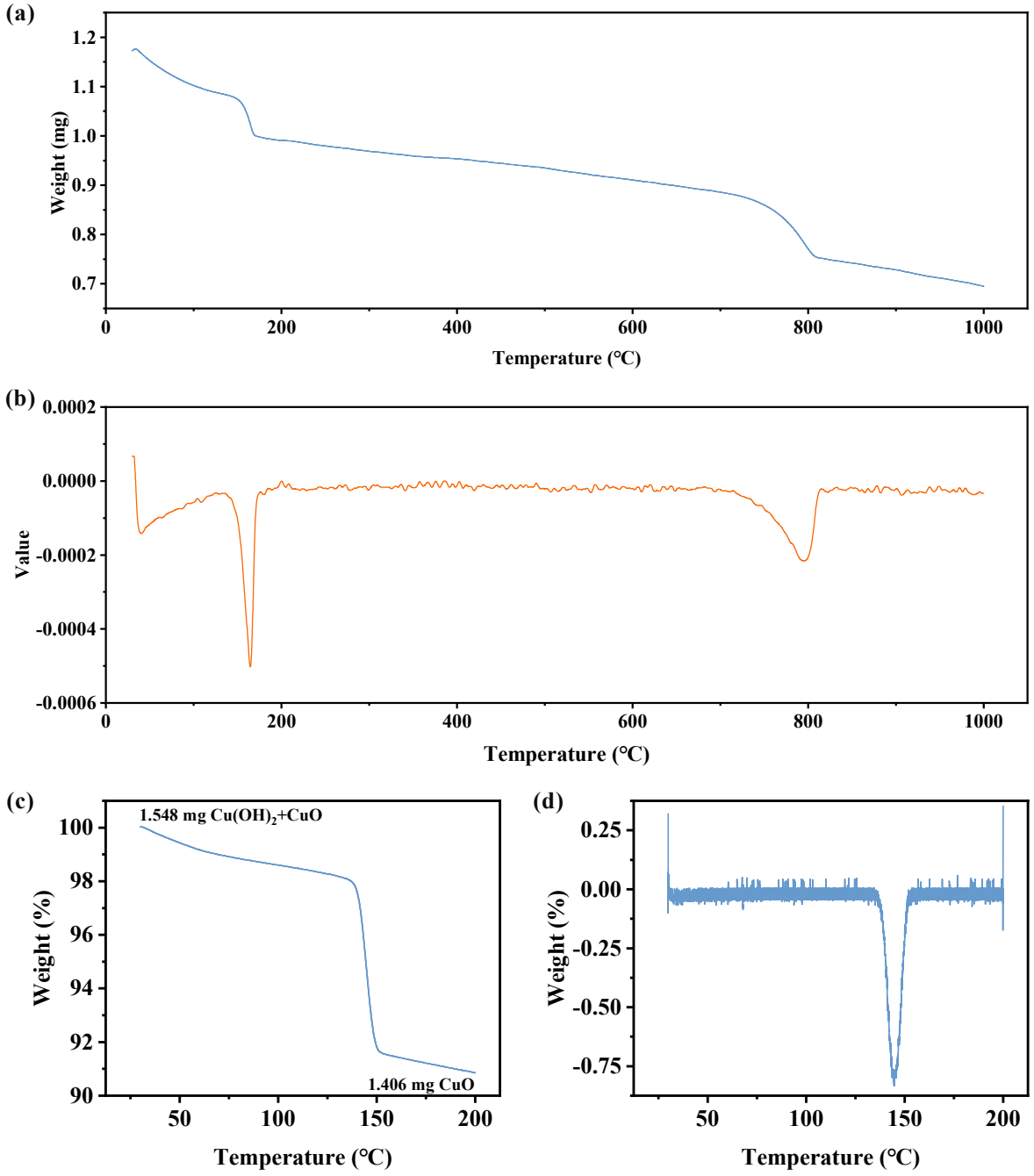

Fig. S14. (**a**) The weight of the sensing materials *vs*. temperature; (**b**) differential coefficient of the weight of the sensing materials *vs*. temperature (25℃~1000℃). (**c**) The weight of the sensing materials *vs* temperature; (**d**) differential coefficient of the weight of the sensing materials *vs* temperature (25℃~200℃).

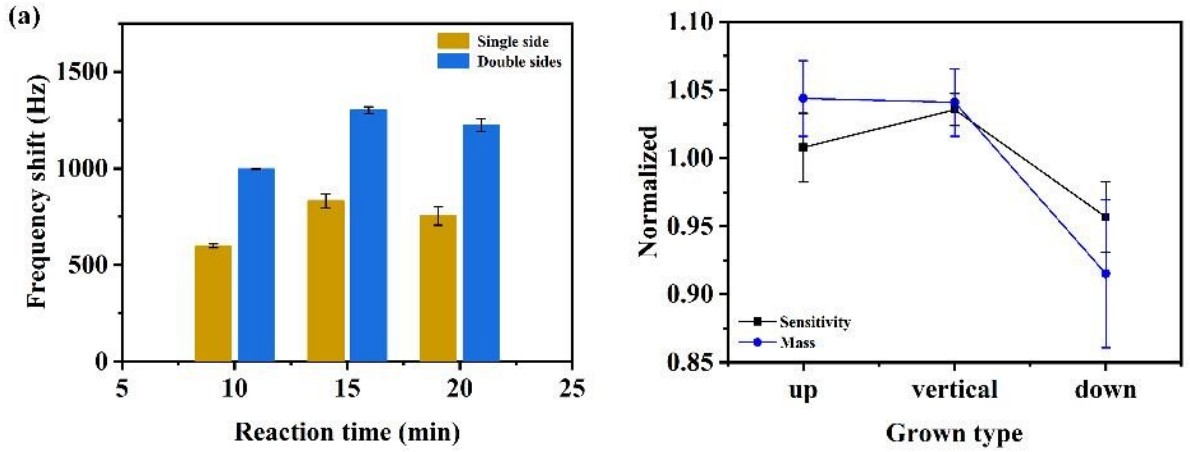

Fig. S15. The performance of the sensor with different (**a**) reaction times and (**b**) growing types.

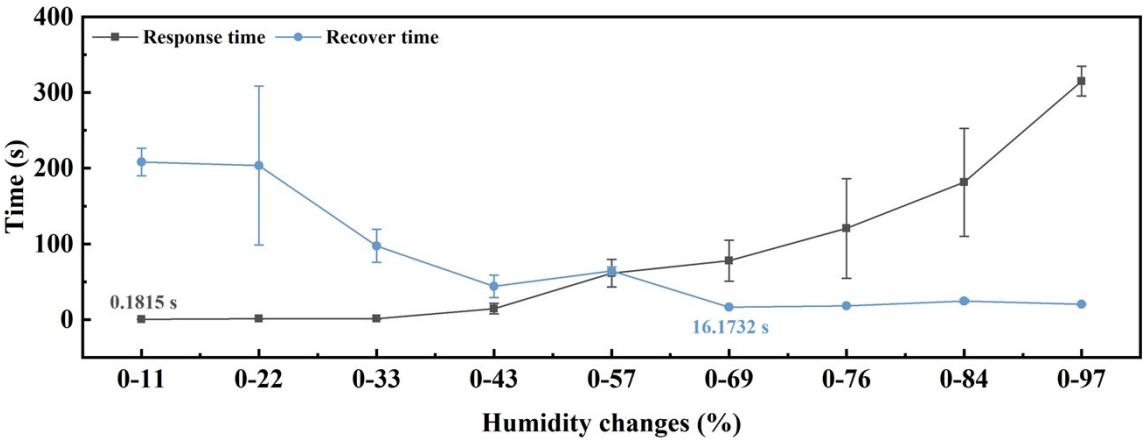

Fig. S16. The response/recovery time of the sensor under different humidity levels.

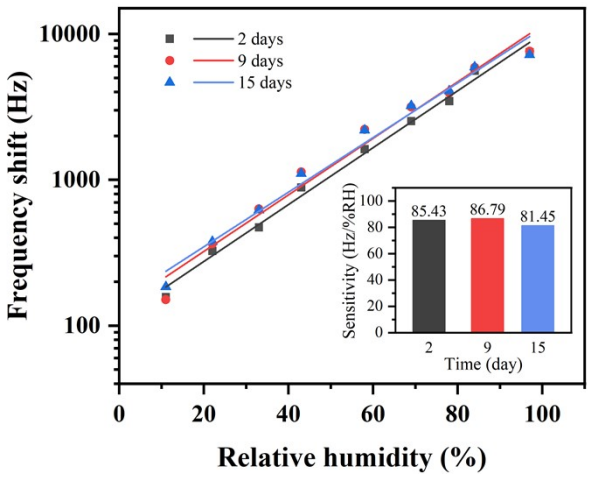

Fig. S17. The response curves of the sensor after long-term storage.

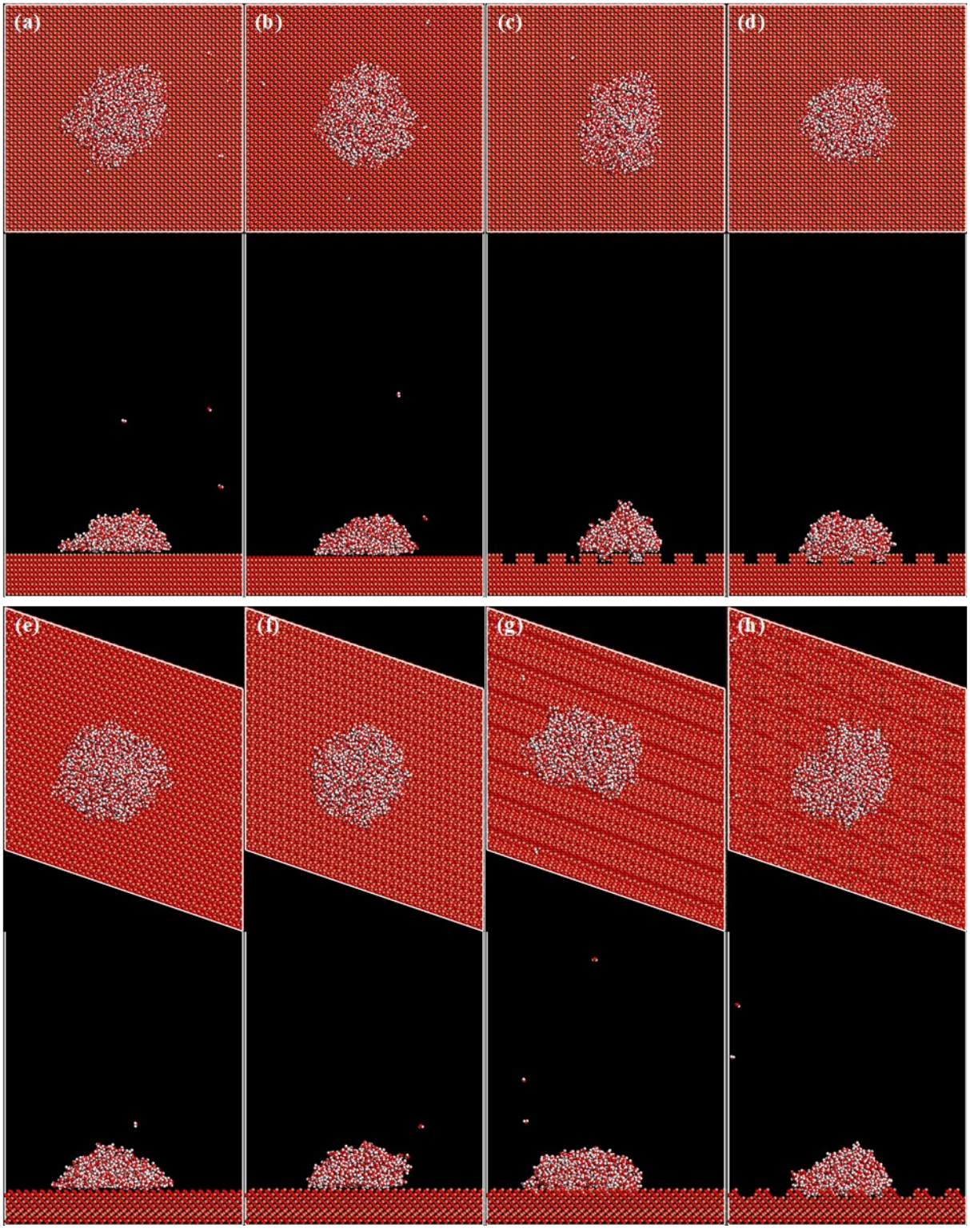

Fig. S18. Water droplet on the (002) CuO surface with (**a**) flat Cu; (**b**) flat O; (**c**) groove array; (**d**) micro-pit array after simulation. Water droplet on the (111) CuO surface with (**e**) flat Cu; (**f**) flat O; (**g**) groove array; (**h**) micro-pit array after simulation.

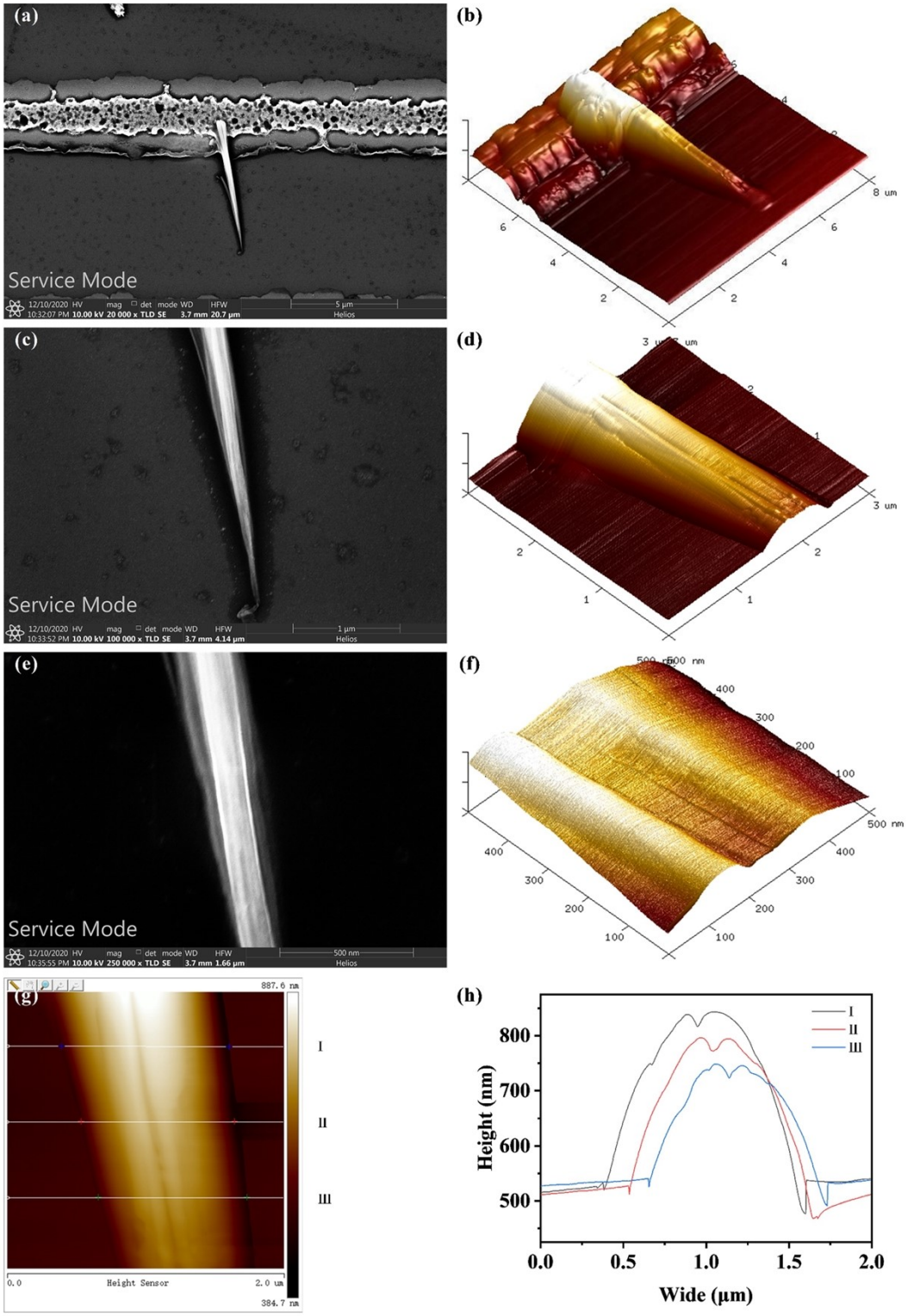

Fig. S19. (**a, c, e**) AFM images and (**b, d, f**) sectional views of the single CuO nanowire at different magnifications; (**g**) Height distribution image of the single CuO nanowire and (**h**) its corresponding sectional height curves.

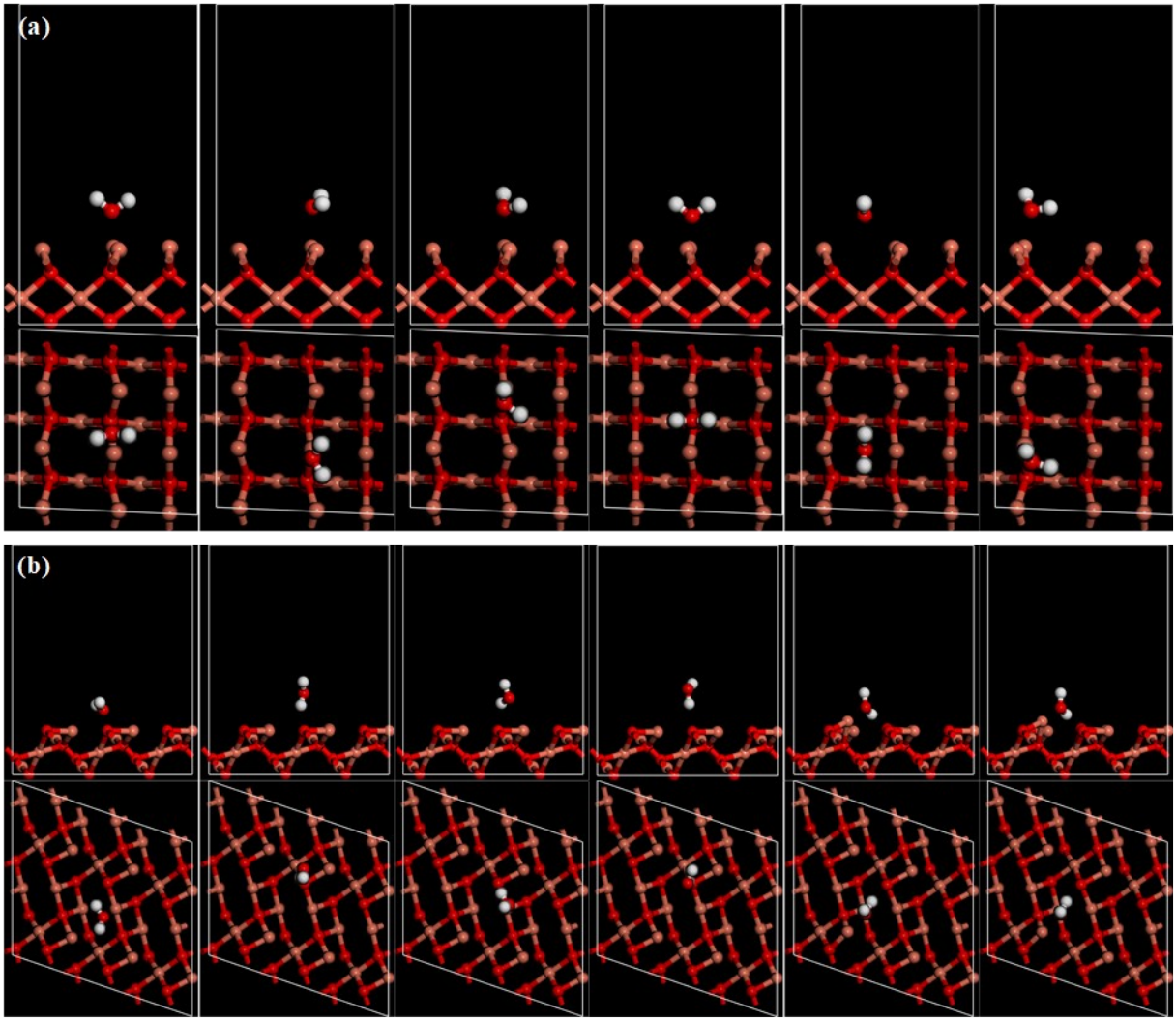

Fig. S20. Adsorption geometries of H_2O on the CuO surfaces after optimized. (**a**) (002); (**b**) (111). The salmon pink, red and gray balls represent Cu, O and H atoms, respectively.

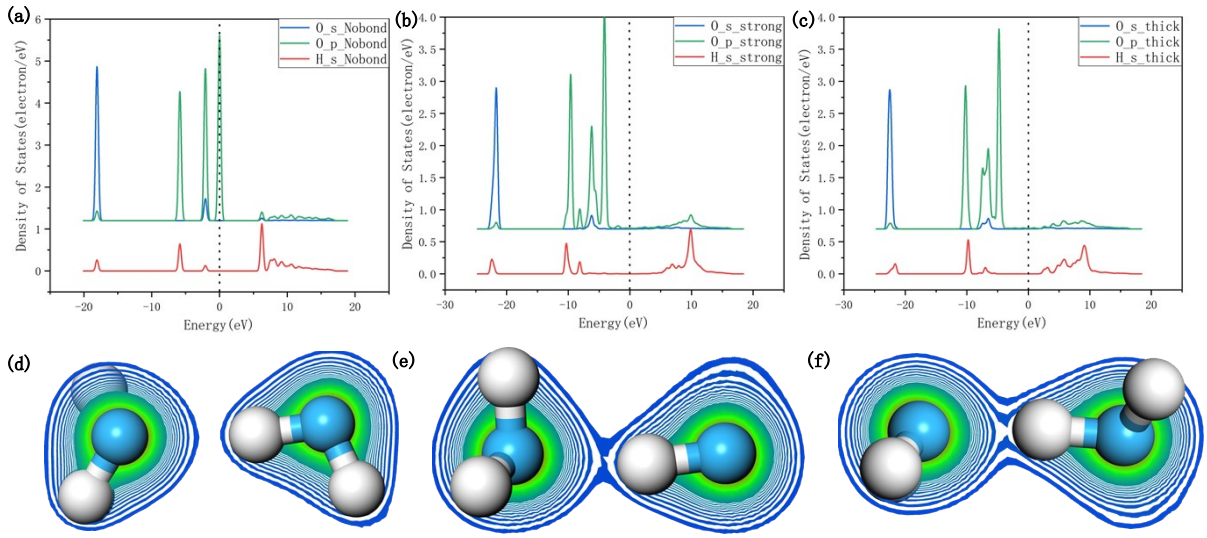

Fig. S21. PDOS of hydrogen bond between two H_2O moleculars (**a**) no hydrogen bond, (**b**) strong hydrogen bond, (**c**) thick hydrogen bond. Charge density distributions of hydrogen bond between two H_2O moleculars (**d**) no hydrogen bond, (**e**) strong hydrogen bond, (**f**) thick hydrogen bond.

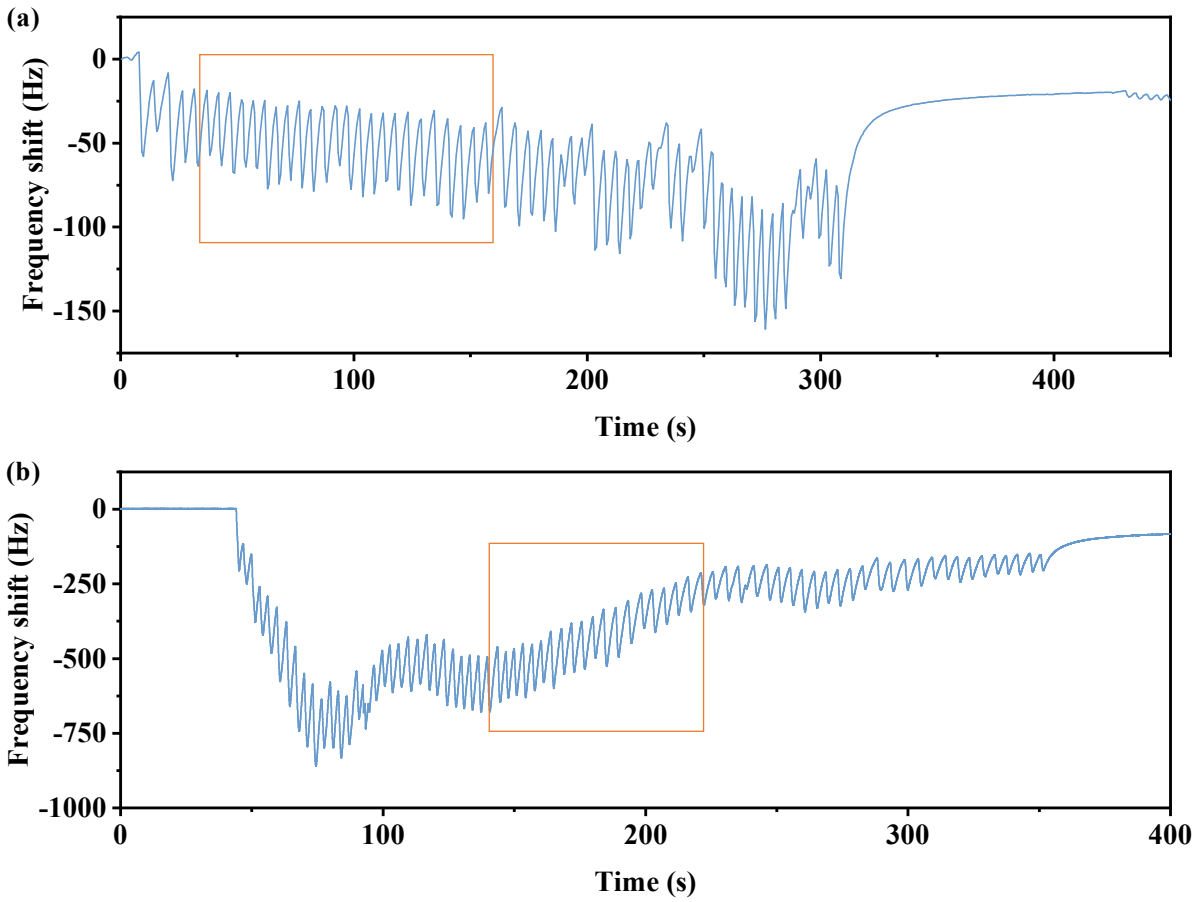

Fig. S22. Human breath (**a**) under normal conditions and (**b**) after sporting.

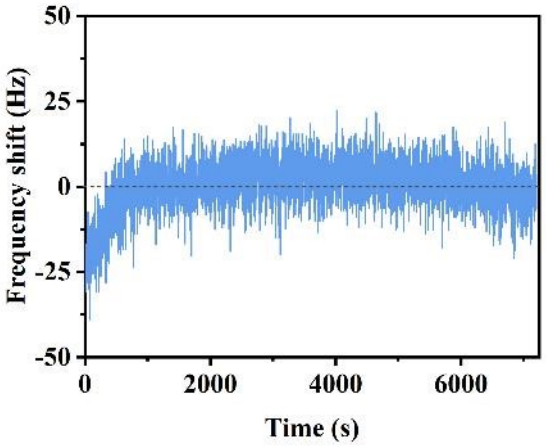

Fig. S23. The robust humidity sensing capability of the CuO nanowires based QCMs.

Table S1. Performance summary of some QCM humidity sensors.

Materials	Sensitivity (Hz/% RH)	Response/recovery time (s)	Ref.
This work	**82.5±7.7**	**0.18/16.17**	—
ND-MXene	82.45	28.00/7.00	*1*
Au@MOF-303	48.27	14.00/15.00	*2*
In_2O_3 QDs	56.3	14.00/16.00	*3*
ZnO nanoneedle	21.4	2.00/2.00	*4*
Hollow ball TiO_2	33.8	5.00/2.00	*5*
$MoS_2/Cu(OH)_2$	60.8	1.90/3.80	*6*
Cu $(OH)_2$	85.9	30.40/1.90	*7*
NCNCs	25.6	18.00/10.00	*8*
PAN/BC NF	64	26.00/24.00	*9*
$MoS_2/GO/C_{60}$-OH	31.8	1.30/1.20	*10*
GO/Carbon	47.61	2.00/2.00	*11*
C_{60}/GO	31.00	34.00/5.00	*12*

Table S2. The water contact angles of different CuO surfaces.

Crystal orientation	Value	Flat-Cu	Flat-O	Groove	Block array
(002)	Average	73.288	72.745	83.347	80.164
	Standard deviation	4.894	1.256	2.378	0.168
(111)	Average	73.528	81.172	76.263	74.203
	Standard deviation	2.928	2.243	7.971	1.930

Adsorption mode	Initial position	Final position	Δeads (ev)	Mode of action	Bond length(a)	Charge transfer amount (ev)	Population
Top-horizontal	Top	Top	-1.078	Covalent adsorption	2.0398	0.16	0.16
Bridge-horizontal	Bridge	Bridge	-1.066	Electrostatic adsorption	2.19561 2.25583	0.12 0.1	0.08 0.06
Hollow-horizontal	Hollow	Hollow	-0.955	Electrostatic adsorption	2.63652 2.25501	0.1 0.13	0.03 0.11
Top-vertical	Top	Top	-1.091	Covalent adsorption	2.03546	0.17	0.2
Bridge-vertical	Bridge	Top	-1.105	Covalent adsorption	2.01777	0.18	0.2
Hollow-vertical	Hollow	Top	-1.053	Covalent adsorption	2.02255	0.16	0.17

Table S3. The adsorption of single-H_2O on different CuO surfaces.

Table S4. The adsorption of mulit- H_2O on different CuO surfaces.

Number of H_2O	ΔEads (eV)	Mode of action and number of bonds	Bond length(A)	population	Adsorption position
1	-1.08/-1.01	covalent bond(1)/Electrostatic adsorption	2.02/2.33	0.18/0.07	top/bridge/hollow
2	-1.57	covalent bond(2)	2.06	0.21	top
3	-1.51	covalent bond(3)	2.33	0.156	top
4	-2.66	covalent bond(2)/Hydrogen bond(2)	2.01/1.63	0.23/0.13	top/between H_2O
8	-5.60	covalent bond(2)/Hydrogen bond(7)	2.08/1.76	0.18/0.10	top/between H_2O

Movie S1. The morphological evolution of droplet bouncing on the obliqued CuO surface with micro-pit.

Movie S2. The self-cleaning process of droplet bouncing on the horizontal CuO surface with micro-pit.

Movie S3. The self-cleaning process of droplet bouncing on the obliqued CuO surface with micro-pit.

Reference

1. Y. Yao, Q. Chen, Y. Li, X. Huang, W. Ling, Z. Xie, J. Wang, C. Chen, Nanodiamond/Ti3C2 MXene-coated quartz crystal microbalance humidity sensor with high sensitivity and high quality factor. *Rare Metals* **43**, 2719-2729 (2024).
2. H. Wang, X. Jia, Z. Ma, X. Wang, X. Zhang, Z. Xue, J. Xu, Incorporating Au nanoparticles into metal-organic framework for low humidity sensors. *Sensors and Actuators B: Chemical* **404**, 135204 (2024).
3. H. Kan, M. Li, H. Li, C. Li, J. Zhou, C. Fu, J. Luo, Y. Fu, A novel quartz-crystal microbalance humidity sensor based on solution-processible indium oxide quantum dots. *RSC Adv.* **9**, 38531-38537 (2019).
4. X. Cha, F. Yu, Y. Fan, J. Chen, L. Wang, Q. Xiang, Z. Duan, J. Xu, Superhydrophilic ZnO nanoneedle array: Controllable in situ growth on QCM transducer and enhanced humidity sensing properties and mechanism. *Sensors and Actuators B: Chemical* **263**, 436-444 (2018).
5. Z. D., C. H., L. P., W. D., Y. Z., Humidity Sensing Properties of Metal Organic Framework-Derived Hollow Ball-Like TiO2 Coated QCM Sensor. *IEEE Sens. J.* **19**, 2909-2915 (2019).
6. J. Lin, H. Fang, X. Tan, B. Sun, Z. Wang, H. Deng, H. Liu, Z. Tang, G. Liao, T. Shi, Ultrafast Self-Assembly MoS2/Cu(OH)2 Nanowires for Highly Sensitive Gamut Humidity Detection with an Enhanced Self-Recovery Ability. *ACS Appl. Mater. Inter.* **11**, 46368-46378 (2019).
7. J. Lin, N. Gao, J. Liu, Z. Hu, H. Fang, X. Tan, H. Li, H. Jiang, H. Liu, T. Shi, G. Liao, Superhydrophilic Cu(OH)2 nanowire-based QCM transducer with self-healing ability for humidity detection. *J. Mater. Chem. A* **7**, 9068-9077 (2019).
8. L. Tang, W. Chen, B. Chen, R. Lv, X. Zheng, C. Rong, B. Lu, B. Huang, Sensitive and renewable quartz crystal microbalance humidity sensor based on nitrocellulose nanocrystals. *Sensors and Actuators B: Chemical* **327**, 128944 (2021).
9. A. Rianjanu, M. Aulya, M. A. A. P. Rayhan, R. Aflaha, S. Maulana, T. Taher, W. S. Sipahutar, M. I. Maulana, N. Yulianto, K. Triyana, H. S. Wasisto, Impact of hydrophilic bamboo cellulose functionalization on electrospun polyacrylonitrile nanofiber-based humidity sensors. *MRS Commun.* **13**, 514-519 (2023).
10. K. Tang, X. Chen, X. Ding, X. Yu, X. Yu, MoS2/Graphene Oxide/C60-OH Nanostructures Deposited on a Quartz Crystal Microbalance Transducer for Humidity Sensing. *ACS Applied Nano Materials* **4**, 10810-10818 (2021).
11. L. Wang, J. Wen, Y. Wu, J. Gao, Graphene Oxide/Carbon Nanocoil Composite for High-performance Humidity Sensor. *Zeitschrift für anorganische und allgemeine Chemie* **646**, 1655-1659 (2020).
12. X. Ding, X. Chen, X. Chen, X. Zhao, N. Li, A QCM humidity sensor based on fullerene/graphene oxide nanocomposites with high quality factor. *Sensors and Actuators B: Chemical* **266**, 534-542 (2018).